

LGIN: Defining an Approximately Powerful Hyperbolic GNN

Srinitish Srinivasan

*School of Computer Science and Engineering
Vellore Institute of Technology*

srinitish.srinivasan2021@vitstudent.ac.in

Omkumar CU

*School of Computer Science and Engineering
Vellore Institute of Technology*

omkumar.cu@vit.ac.in

Abstract

While graph neural networks (GNNs) operating in hyperbolic spaces have shown promise for modeling hierarchical and complex relational data, a critical limitation often overlooked is their potentially limited discriminative power compared to their Euclidean counterparts or fundamental graph isomorphism tests like the Weisfeiler-Lehman (WL) hierarchy. Existing hyperbolic aggregation schemes, while curvature-aware, may not sufficiently capture the intricate structural differences required to robustly distinguish non-isomorphic graphs owing to non-injective aggregation functions. To address this expressiveness gap in hyperbolic graph learning, we introduce the Lorentzian Graph Isomorphic Network (LGIN), a novel GNN designed to achieve enhanced discriminative capabilities within the Lorentzian model of hyperbolic space. LGIN proposes a new update rule that effectively combines local neighborhood information with a richer representation of graph structure designed to preserve the Lorentzian metric tensor. This represents a significant step towards building more expressive GNNs in non-Euclidean geometries, overcoming a common bottleneck in current hyperbolic methods. We conduct extensive evaluations across nine diverse benchmark datasets, including molecular and protein structures. LGIN consistently outperforms or matches state-of-the-art hyperbolic and Euclidean GNNs, showcasing its practical efficacy and validating its superior ability to capture complex graph structures and distinguish between different graphs. To the best of our knowledge, LGIN is the first work to study the framework behind a powerful GNN on the hyperbolic space. The code for our paper can be found at <https://github.com/Deceptrax123/LGIN>

1 Introduction

Graphs constitute an abstract concept for modeling relationships and structures across diverse scientific and technological domains comprising of social networks(Li et al., 2023), biological systems(Zhang et al., 2021b) and knowledge graphs(Ye et al., 2022). Extracting representational information from graphs by mapping such abstraction to coordinate spaces is critical for downstream tasks such as node classification(Zhao et al., 2021), link prediction(Yun et al., 2021) and graph classification(Xie et al., 2022). Graph Neural Networks ((Kipf & Welling, 2016),(Veličković et al., 2017),(Hamilton et al., 2017)) have achieved notable success in these areas by employing a scheme of feature transformation followed by neighbor aggregation. However, these methods significantly operate in Euclidean spaces, potentially overlooking the hierarchical and multi-relational characteristics inherent to complex graphs.

The limitations of Euclidean space for modeling graphs with hierarchical and multi-scale structures have motivated researchers to explore alternative geometries. Hyperbolic geometry, in particular, has emerged as a promising alternative for graph representation learning. Unlike Euclidean space, hyperbolic space grows exponentially in volume with radius, making it naturally suited for embedding hierarchical data with minimal distortion (Zhu et al., 2023). This property enables hyperbolic embeddings to more accurately capture

arXiv:2504.00142v3 [cs.LG] 5 May 2025

the intricate relationships present in hierarchical data, such as taxonomies, protein-protein interaction networks, and social hierarchies. Additionally, hyperbolic geometry requires fewer dimensions to represent such structures effectively, resulting in improved computational efficiency and better preservation of structural information (Zhang et al., 2021a).

In parallel, the theoretical framework of Graph Isomorphic Networks (GINs) (Xu et al., 2018) has gained attention due to its ability to capture structural features of graphs and distinguish non-isomorphic graphs. GINs leverage injective aggregation mechanisms and readout functions to ensure that distinct graph structures map to different embeddings, making them as powerful as the Weisfeiler-Lehman (WL) test for graph isomorphism. This has made GINs a popular choice for tasks requiring high expressivity, such as molecular property prediction and community detection. Despite the successes of GINs in Euclidean space, there is a notable absence of such frameworks adapted for hyperbolic spaces, which could potentially unlock even greater representational power by harnessing the unique properties of hyperbolic geometry.

However, extending such frameworks to the hyperbolic space is inherently challenging due to the need to ensure that embeddings remain constrained within the Riemannian manifold. In particular, ensuring that the operations performed during aggregation and transformation preserve the hyperbolic metric is non-trivial. Motivated by the potential to unify high expressive power with geometry suited for hierarchical data, we propose the Lorentzian Graph Isomorphic Network (LGIN). Our design prioritizes maintaining the intrinsic geometric properties and preserving the Lorentzian metric during aggregation and transformation, which presents challenges for achieving strictly injective message-passing. To effectively bridge this expressiveness gap, LGIN introduces a novel node update rule incorporating a cardinality-aware aggregation mechanism. This design is specifically crafted to approximate the strong discriminative capabilities associated with Euclidean Graph Isomorphism Networks (GINs) by preserving crucial information often lost in standard hyperbolic aggregations. Our empirical results demonstrate that LGIN achieves superior discriminative capabilities compared to existing hyperbolic GNNs, including LGCN and other architectures. We further provide a key contribution by empirically demonstrating that the proposed Hyperbolic-Tangent-Hyperbolic approach, when coupled with cardinality-aware aggregation, yields a GNN with expressivity at least approximately equivalent to the 1-dimensional Weisfeiler-Lehman test. By rigorously integrating structural isomorphism testing principles with the inherent geometric inductive biases of hyperbolic space, this work establishes a foundational theoretical framework for designing powerful and highly-discriminative GNNs on non-Euclidean manifolds.

Therefore, we summarize our key contributions as follows:

- To the best of our knowledge, **this is the first study that makes an attempt to study an isomorphic Graph Neural Network(GNN)** that incorporates both constant and variable curvature information.
- We show that GNNs built using the **hyperbolic-tangent-hyperbolic approach while preserving the metric tensor at the origin has high discriminative capability.**
- We propose the theoretical framework for **Lorentzian Graph Isomorphic Network(LGIN)**, with **a modified cardinality-scaled aggregation rule to preserve the cardinality information of multisets and a new update rule**, as an approximately powerful alternative to Graph Isomorphic Network(GIN) and other state of the art hyperbolic graph neural networks such as LGCN.
- We conduct several experiments across 9 benchmark datasets ranging from MoleculeNet to TU benchmarks and show that our approach consistently outperforms or matches most baselines.

2 Related Work

In this section we describe the related work with respect to Hyperbolic GNNs, mathematical frameworks explaining powerful GNNs and applications of hyperbolic graph neural networks.

2.1 Advances in Hyperbolic Graph Neural Networks

Hyperbolic graph neural networks, as discussed above, have emerged as a powerful method for modeling complex and hierarchical structures. (Liu et al., 2019) generalized graph neural networks to be manifold-agnostic and demonstrated that hyperbolic graph neural networks are more efficient at capturing structural properties than their Euclidean counterpart. (Khatir et al., 2022) proposed the Poincare disk model as the search space to apply all approximations on the disk, thus eliminating the need for inter-space transformations. This framework introduces a hyperbolic normalization layer that simplifies the entire hyperbolic model to a Euclidean model cascaded with the normalization layer, maintaining the advantages of both geometric approaches. (Fu et al., 2023) introduced ACE-HGNN which dynamically learns the optimal curvature based on the input graph and downstream tasks. Using a multi-agent reinforcement learning framework with two agents—ACE-Agent and HGNN-Agent—for learning curvature and node representations respectively, this model adapts to the specific hierarchical structures present in different graphs rather than using a manually fixed curvature value. (Zhang et al., 2021a) introduced Lorentzian Graph Convolutional Networks(LGCN) for modeling hierarchical architectures. They design a neighborhood aggregation method based on the centroid of Lorentzian distance to constrain embeddings within the hyperboloid. Further, they theoretically prove that some proposed graph operations are equivalent to those defined in other hyperbolic models such as the Poincare ball model. (Choudhary et al., 2023) introduced H-GRAM, a meta-learning framework specifically designed for hyperbolic graph neural networks. The model learns transferable information from local subgraphs in the form of hyperbolic meta gradients and label hyperbolic protonets thereby enabling faster learning over new tasks dealing with disjoint subgraphs, thus addressing the generalization challenge.

2.2 Applications of Hyperbolic Graph Neural Networks

(Ramirez et al., 2025) used a Fully Hyperbolic Graph Neural Network(FHGNN) to embed functional brain connectivity graphs derived from magnetoencephalography (MEG) data into low dimensions on a Lorentz model of hyperbolic space. (Wu et al., 2021) developed a graph-based Quantitative Structure-Activity Relationship(QSAR) method by building a hyperbolic relational graph convolution network. It leverages both molecular structure and molecular descriptors to achieve state-of-the-art performance on 11 drug discovery-related datasets. (Bao et al., 2025) introduced Hyperbolic Graph Convolutional Network-based Knowledge Graph Embedding (HGCGE) which addresses challenges in traditional GCN-based KGE methods, such as oversmoothing and high distortion in Euclidean space. It employs GCN operations in hyperbolic space with Möbius transformations to embed entities and relationships in the Poincaré model, enhancing hierarchical data representation. The proposed scoring function improves entity distinction across relationships, achieving superior performance on multiple datasets, even at low dimensions and training rounds.

2.3 Graph Expressiveness

(Xu et al., 2018) presented a theoretical framework for analyzing the expressive power of GNNs. Their analysis demonstrated that popular GNN variants such as Graph Convolutional Networks and GraphSAGE cannot distinguish certain simple graph structures, limiting their discriminative capabilities. The researchers then developed a simple architecture—the Graph Isomorphism Network—that is provably the most expressive among the class of message-passing GNNs and as powerful as the 1-dimensional Weisfeiler-Lehman(WL) graph isomorphism test. (Hevathige & Wang, 2023) showed that partitioning a graph into sub-graphs that preserve structural properties provides a powerful means to exploit interactions among different structural components of the graph. The researchers proposed Graph Partitioning Neural Networks(GPNNs) that combines structural interactions via permutation invariant graph partitioning to enhance graph representation learning.

3 Preliminaries

In this section, we formally define the key terms and establish the theoretical framework underlying our proposed work. For a deeper understanding of geometric topology, refer to (Martelli, 2016).

3.1 Graph Preliminaries

Graph. Consider the definition of a Graph $G = (V, E)$. Let V be the set of vertices $\{v_1, v_2, \dots, v_{n_v}\}$ and E be the set of edges $\{e_1, e_2, \dots, e_{n_e}\}$. n_v, n_e are the number of vertices and edges in G respectively. Each vertex v is characterized by an initial n dimensional vector depending on the problem set. The problem set may be a set of molecular graphs, protein networks, citation networks etc.

Weisfeiler-Lehman(WL) Test. The Weisfeiler-Lehman (WL) test is a graph isomorphism heuristic that iteratively refines node representations based on local neighborhood aggregation. Given a graph, the test assigns initial labels to nodes and updates them iteratively by incorporating labels from neighboring nodes. This process continues until convergence, producing a unique representation for each node that captures its structural role within the graph (Morris et al., 2019). The WL test is widely used to distinguish non-isomorphic graphs efficiently and serves as a foundation for many graph neural networks (GNNs) (Xu et al., 2018).

3.2 Definitions of Key Topological Concepts

Definition 3.1 (Differential Manifold). A differential manifold is a topological space \mathcal{M} that is locally homeomorphic to \mathbb{R}^n and consists of a smooth structure that allows for the differentiation of functions. In other words, there is a covering $\{U_i\}$ of \mathcal{M} consisting of open sets U_i homeomorphic to open sets V_i in \mathbb{R}^n .

Definition 3.2 (Tangent Space). Let \mathcal{M} be a differential manifold of dimension n . We define for every point $p \in \mathcal{M}$ a n dimensional vector space $T_p\mathcal{M}$ called the tangent space. The space $T_p\mathcal{M}$ may be defined briefly as the set of all curves $\gamma : (-a, a) \rightarrow \mathcal{M}$ such that $\gamma(0) = p$ and $a > 0$ is arbitrary, considered up to some equivalence relation. The relation is that we identify two curves, that read on some chart (U_i, φ) have the same tangent vector at $\varphi_i(p)$. The relationship between the hyperbolic space and the corresponding tangent space is called a map.

Definition 3.3 (Metric Tensor). A metric tensor on a differentiable manifold \mathcal{M} assigns a smoothly varying inner product to each tangent space $T_p\mathcal{M}$ at every point $p \in \mathcal{M}$. A metric tensor on \mathcal{M} is a smooth, symmetric, bilinear map

$$g : T\mathcal{M} \times T\mathcal{M} \rightarrow \mathbb{R}$$

such that for each point $p \in \mathcal{M}$, the restriction g_p to the tangent space $T_p\mathcal{M}$ satisfies:

$$g_p(X, Y) = g_p(Y, X), \quad \forall X, Y \in T_p\mathcal{M},$$

where g_p is a symmetric, positive-definite bilinear form. This tensor defines an inner product structure on each tangent space, allowing the measurement of angles, lengths, and distances on \mathcal{M} . Based on this, we can define that the Riemannian manifold is a differentiable manifold with a metric tensor that is positive semi-definite at every point.

Definition 3.4 (Curvature). The curvature of a Riemannian manifold (\mathcal{M}, g) is a mathematical entity that measures how distorted the metric tensor g is when compared to the Euclidean structure on \mathbb{R}^n . Let (\mathcal{M}, g) be a Riemannian manifold, where g is the metric tensor. The Riemann curvature tensor is defined as

$$R(X, Y)Z = \nabla_X \nabla_Y Z - \nabla_Y \nabla_X Z - \nabla_{[X, Y]} Z, \quad (1)$$

for vector fields X, Y, Z on \mathcal{M} , where ∇ is the Levi-Civita connection.

The sectional curvature at a point p for a 2-plane σ spanned by $\{X, Y\}$ in the tangent space $T_p\mathcal{M}$ is given by

$$K(X, Y) = \frac{\langle R(X, Y)Y, X \rangle_g}{\|X\|_g^2 \|Y\|_g^2 - \langle X, Y \rangle_g^2}. \quad (2)$$

For a Lorentzian space with constant curvature K , the Riemann tensor satisfies

$$R(X, Y)Z = K (\langle Y, Z \rangle_g X - \langle X, Z \rangle_g Y). \quad (3)$$

Definition 3.5 (Isometry). A diffeomorphism $f : \mathcal{M} \rightarrow \mathcal{N}$ between two Riemannian manifolds (\mathcal{M}, g) and (\mathcal{N}, h) is an isometry if it preserves the scalar product i.e., the equality,

$$\langle v, w \rangle = \langle df_p(v), df_p(w) \rangle \quad (4)$$

holds for all $p \in \mathcal{M}$ and every pair of vectors $v, w \in T_p\mathcal{M}$. The symbol \langle, \rangle indicates the scalar products in $T_p\mathcal{M}$ and $T_{f(p)}\mathcal{N}$.

Definition 3.6 (Parallel Transport). Parallel transport is a geometric operation that moves a vector along a curve on a manifold while preserving its inner product with tangent vectors along the path. In the context of hyperbolic geometry, parallel transport ensures that vectors remain tangent to the hyperboloid model while accounting for the manifold's curvature. It is a way to slide frames along geodesics.

3.3 Hyperboloid Model

In the hyperboloid model, we define \mathbb{H}^n as the set of all points of norm -1 in \mathbb{R}^{n+1} , equipped with the Lorentzian scalar product. The Lorentzian scalar product on \mathbb{R}^{n+1} is given by

$$\langle x, y \rangle_\eta = -x_0y_0 + \sum_{i=1}^n x_iy_i \quad (5)$$

The Lorentz model of the hyperbolic space, is formally defined as follows:

$$\mathbb{H}^n = \{x \in \mathbb{R}^{n+1} \mid \langle x, x \rangle_\eta = -1, x_0 > 0\} \quad (6)$$

The set of points x with $\langle x, x \rangle_\eta = -1$ is a hyperboloid with two sheets. As mentioned earlier, maps form the relationship between the hyperbolic space and the corresponding tangent space. Formally, for a point $p \in \mathcal{M}$, the exponential map

$$\exp_p : T_p\mathcal{M} \longrightarrow \mathcal{M}$$

is defined as follows: A vector $v \in T_p\mathcal{M}$ determines a maximal geodesic $\gamma_v : \mathbb{R} \rightarrow \mathcal{M}$ with $\gamma_v(0) = p$ and $\gamma'_v(0) = v$. We set $\exp_p(v) = \gamma_v(1)$. The logarithmic map \log_p is the inverse of the exponential map. In the hyperboloid space, the exponential and logarithmic maps are given by equations 7 and 8 respectively.

$$\exp_p(v) = \cosh\left(\sqrt{|c|}\|v\|_\eta\right)p + \sinh\left(\sqrt{|c|}\|v\|_\eta\right)\frac{v}{\|v\|_\eta} \quad (7)$$

where $p \in \mathbb{H}^n$, c is the curvature and $v \in T_p\mathbb{H}^n$ is a tangent vector at p .

$$\log_p(q) = \frac{d_{\mathbb{H}}(p, q)}{\sinh\left(\sqrt{|c|}d_{\mathbb{H}}(p, q)\right)}\left(q - \cosh\left(\sqrt{|c|}d_{\mathbb{H}}(p, q)\right)p\right) \quad (8)$$

where

$$d_{\mathbb{H}}(p, q) = \frac{1}{\sqrt{|c|}}\cosh^{-1}(-\langle p, q \rangle_\eta) \quad (9)$$

is the hyperbolic distance in the Lorentzian space. The parallel transport is given by:

$$PT_{p \rightarrow q}^c(v) = v - \frac{c\langle q, v \rangle_\eta}{1 + c\langle p, q \rangle_\eta}(p + q) \quad (10)$$

4 Proposed Framework

In this section, we discuss the framework for an approximately powerful GNN on the Lorentzian model. Note that this can be extended to other hyperbolic models as well through their respective exponential and logarithmic maps. We discuss the properties of the manifold that allow for discriminative GNNs, however such frameworks are limited by the need of preserving the metric tensor and attention aggregated weights. Throughout our study, we consider more importance to metric tensor preservation than injectivity of aggregation.

4.1 Overview

Theorem 4.1 (Manifold Property for powerful GNNs). *Let $G_1 = (V_1, E_1)$ and $G_2 = (V_2, E_2)$ be two graphs. Consider a smooth Lorentzian manifold (\mathcal{M}, g) of constant negative curvature $c < 0$, where g is the Lorentzian metric tensor. Suppose there exists an embedding*

$$\Phi : \mathcal{G} \rightarrow \mathcal{M} \quad (11)$$

that maps vertices of any graph $G \in \mathcal{G}$ into the hyperboloid model \mathbb{H}^n and preserves graph structural properties (e.g., graph distance) through the Lorentzian distance on \mathcal{M} . If G_1 and G_2 are non-isomorphic, then their embeddings $\Phi(G_1)$ and $\Phi(G_2)$ cannot be related by a global isometry f of (\mathcal{M}, g) , i.e., there does not exist a diffeomorphism

$$f : \mathcal{M} \rightarrow \mathcal{M} \quad (12)$$

such that

$$f^*g = g \quad \text{and} \quad f \circ \Phi(G_1) = \Phi(G_2) \quad (13)$$

We present the proof for theorem 4.1 in appendix A. Therefore, we can demonstrate that a graph neural network mapping node features onto a hyperboloid can achieve representational power approximately comparable to the Weisfeiler-Lehman (WL) test owing to the property of the metric embeddings on a hyperbolic manifold, thus describing a desirable embedding. However, the following must be taken into consideration:

- A powerful graph neural networks requires strictly injective aggregation and readout functions (Xu et al., 2018). However, directly translating strictly injective operations to Riemannian manifolds while preserving geometric properties is non-trivial. Our goal is to design a network that achieves high expressive power by carefully approximating these properties within the Lorentzian geometry.
- Additionally, geometric consistency i.e the preservation of metric tensors of the hyperboloid model needs to be ensured.

To account for the above considerations, we have provided a detailed explanation in the following sections.

4.2 Injectivity of Lorentz Transformation

We show the injectivity of the Lorentz Transformation on the manifold and through moment injectivity proposed by (Amir et al., 2023). To ensure the injectivity of the Lorentz transformation, we follow the hyperbolic-tangential-hyperbolic approach (Zhang et al., 2021a). This is because the tangent space at a point is locally isometric to Euclidean space. The Lorentz transformation used in our proposed method is given by:

$$\mathbf{W} \otimes_c^{\mathcal{L}} \mathbf{x}^{\mathcal{L}} := \exp_o^c \left(0, \mathbf{W} \log_o^c \left(\mathbf{x}^{\mathcal{L}} \right)_{[1:n]} \right), \quad (14)$$

where $\mathbf{x}^{\mathcal{L}} \in \mathcal{L}_c^n$, $\mathbf{W} \in \mathbb{R}^{d \times n}$. This method ensures the first coordinate is consistently zero, signifying that the resultant transformation is invariably within the tangent space at \mathbf{o} . In the following sections. we prove the injectivity of the Lorentz transformation.

4.2.1 Injectivity on the Manifold

Proposition 4.2. *The Lorentzian transformation $\mathbf{W} \otimes_c^{\mathcal{L}} : \mathcal{H}^n \rightarrow \mathcal{H}^d$ defined by*

$$\mathbf{W} \otimes_c^{\mathcal{L}} x^{\mathcal{L}} = \exp_o^c \left(0, \mathbf{W} \left(\log_o^c x^{\mathcal{L}} \right)_{[1:n]} \right)$$

is injective if and only if the weight matrix $\mathbf{W} \in \mathbb{R}^{d \times n}$ has full column rank, i.e., $\text{rank}(\mathbf{W}) = n$. This requires $d \geq n$.

The proof of the above proposition is detailed in appendix B. Based on proposition 4.2, we ensure that the transformation matrix \mathbf{W} has a full column rank by setting the number of output dimensions to be greater than the number of input dimensions for each layer.

4.2.2 Moment Injectivity

From (Amir et al., 2023), we have the following result for the Euclidean space: Consider shallow neural networks $f : \mathbb{R}^d \rightarrow \mathbb{R}^m$ of the form

$$f(\mathbf{x}; A, \mathbf{b}) = \sigma(A\mathbf{x} + \mathbf{b}), \quad A \in \mathbb{R}^{m \times d}, \quad \mathbf{b} \in \mathbb{R}^m, \quad (15)$$

with the activation function $\sigma : \mathbb{R} \rightarrow \mathbb{R}$ applied entrywise to $A\mathbf{x} + \mathbf{b}$. Suppose that σ is analytic and non-polynomial; such activations include the sigmoid, softplus, tanh, swish, and sin. For a large enough m , such networks $f(\mathbf{x}; A, \mathbf{b})$ with random parameters A, \mathbf{b} are moment-injective on $\mathcal{M}_{\leq n}(\Omega)$ and on $\mathcal{S}_{\leq n}(\Omega)$; namely, their induced moment functions \hat{f} are injective. This holds for various natural choices of Ω . \hat{f} is given by $f : \Omega \rightarrow \mathbb{R}^m$ that induces a moment function

$$\hat{f} : \mathcal{M}_{\leq n}(\Omega) \rightarrow \mathbb{R}^m$$

defined by

$$\hat{f}(\mu) = \int_{\Omega} f(x) d\mu(x) = \sum_{i=1}^n w_i f(x_i), \quad \text{where } \mu = \sum_{i=1}^n w_i \delta_{x_i}. \quad (16)$$

Now, extending the theory from eq.16 to the hyperboloid, we have the transformation defined in eq.14, where $x^{\mathcal{L}}$ is first mapped to the tangent space. We already know that the tangent space at a point is locally isometric to the Euclidean space. Therefore, by the isometry, the moment function in this transformed space becomes:

$$\hat{f}(\mu) = \int_{\mathcal{L}_c} f(\mathbf{x}^{\mathcal{L}}) d\mu(\mathbf{x}^{\mathcal{L}}) = \sum_{i=1}^n w_i f(\mathbf{x}_i^{\mathcal{L}}), \quad \mu = \sum_{i=1}^n w_i \delta_{\mathbf{x}_i^{\mathcal{L}}}. \quad (17)$$

Therefore, we use a shallow(2-Layer) Lorentzian network based on transformation equation 14 with a point-wise Tanh/Sigmoid function and ensuring \mathbf{W} has a full column rank.

4.3 Lorentzian Graph Isomorphic Network

Based on the conditions mentioned in section 4.1, proof in section 4.2 and corollary 6 in (Xu et al., 2018), we finally define the update rule for the Lorentzian Graph Isomorphic Network(LGIN) as follows:

$$\mathbf{x}^{\mathcal{L}^k} = \text{LT}^k(\exp_o^c((1 + \epsilon^k) \cdot \mathcal{P}_{x^{\mathcal{L}^{k-1}}} \rightarrow_T(\log_o^c(\mathbf{x}^{\mathcal{L}^{k-1}})) + \log_o^c(T(\mathbf{x}^{\mathcal{L}^{k-1}})))) \quad (18)$$

where $\mathbf{x}^{\mathcal{L}}$ is a point in the Lorentzian space, LT represents the Lorentz transformation which is a 2-layer model with Tanh activation and output features greater than input, k is the step and T is the output of neighbor aggregation given by the cardinality aware Lorentz centroid method as follows:

$$T(\mathbf{x}_i^{\mathcal{L}^{k-1}}) := \frac{\sqrt{c} \sum_{j \in \mathcal{N}_i} \alpha_{ij} \mathbf{x}_j^{\mathcal{L}}}{(1 + |\mathcal{N}_i|) \|\sum_{j \in \mathcal{N}_i} \alpha_{ij} \mathbf{x}_j^{\mathcal{L}}\|_{\mathcal{L}}} \quad (19)$$

where α_{ij} refers to weights with squared hyperbolic distance to lay emphasis on geometry. It is given by:

$$\alpha_{ij} = \text{softmax}_{j \in \mathcal{N}(i)}(-d_c^2(\mathbf{x}_i^{\mathcal{L}}, \mathbf{x}_j^{\mathcal{L}})) \quad (20)$$

4.3.1 Justification of Lorentz Centroid

Equation 19 ensures embeddings reside on the hyperbolic manifold after aggregation i.e the preservation of metric tensors. Normalization prevents the node embeddings from collapsing into the origin or drifting too far. However, since attention-based aggregators are not strictly injective, it may lead to non-isomorphic graphs having the same embeddings. To mitigate this, we modify the Lorentz aggregation function to preserve the cardinality information of multisets during aggregation which can approximate the injective property(Zhang & Xie, 2020).

4.3.2 Justification of Parallel Transport

Parallel Transport in equation 18 preserves the hyperbolic structure and avoids distorting embeddings. The embeddings of two neighboring nodes reside in different tangent spaces because each node has its own local geometry due to curvature. A direct aggregation of features between nodes would lead to the mixing of incompatible spaces, thereby leading to node representations that are not completely representative of that node. We provide an empirical analysis by comparing the model’s performance with and without parallel transport in the following section.

5 Experiments

In this section, we discuss the experimental conditions and results obtained from testing the Lorentzian Graph Isomorphic Network over various datasets.

5.1 Experimental conditions

5.1.1 Datasets

For our experiments, we use 6 Bioinformatics datasets and 3 MoleculeNet datasets. The bioinformatics datasets include, namely, Proteins, Mutag, NCI1, PTC, Enzymes, and DD(Yanardag & Vishwanathan, 2015). The MoleculeNet datasets include, namely, BBBP, BACE and HIV(Wu et al., 2018). The initial features of the Bioinformatics datasets are mostly the node degree, while for MoleculeNet, each node is assigned 9 features such as atomic number, chirality, formal charge, or whether the atom is in a ring or not.

5.1.2 Hyperparameters and model configuration

In our proposed method, we evaluate on sets of variants. One with a constant curvature c and the other with variable curvature, which is essentially a trainable parameter. All initial curvatures were set to 4. The trainable parameter ϵ was initially set to 0.1. We use the Riemannian Adam(Bécigneul & Ganea, 2018) to train our model with a cosine annealing learning rate scheduler with warm restarts. We use the same model architecture for all datasets, which is a 3-layer Lorentzian Graph Isomorphic Network predicting 128, 256 and 512 features respectively. To ensure stability of gradient flow, we make use of gradient clip after gradient computation at each step. The number of Lorentz Transformation layers have been set to 2.

5.2 Evaluations

In this section, we compare our framework against several baselines as mentioned in the previous section. We mainly compare our model with Graph Isomorphic Network(GIN), a powerful GNN framework defined for the Euclidean space and its variants. Unless otherwise mentioned, for Bioinformatics datasets, we record the mean and standard deviation of the test accuracy on 10 splits. For MoleculeNet datasets, we consider the average accuracy on 3 splits.

5.2.1 Evaluations against Graph Isomorphic Network

Table 1 contains the performance of our model against powerful baselines. The performance of various GNN variants against LGIN was evaluated across four datasets: MUTAG, PROTEINS, PTC, and NCI1. The proposed LGIN variants demonstrate competitive performance across diverse datasets. Notably, **LGIN with Fixed Curvature** achieves the highest accuracy on the **MUTAG** dataset (90.6 ± 3.9) and the **PTC** dataset (68.4 ± 5.2), outperforming several existing models. Furthermore, **LGIN with Variable Curvature** attains the best performance on the **PROTEINS** dataset (79.1 ± 4.4), showing statistically significant improvement ($p < 0.1$). In the case of the **NCI1** dataset, the Weisfeiler-Lehman (WL) subtree kernel achieved the best performance with 86.0 ± 1.8 , while the PATCHYSAN model showed competitive performance on the MUTAG dataset with 92.6 ± 4.2 . Across other datasets, several GIN variants such as SUM-MLP (GIN- ϵ) and SUM-1-LAYER also reported consistent results. The performance gains observed in LGIN, particularly in datasets with varying node sizes and graph complexities, underscore its ability to effectively

Table 1: **Performance of GNN Variants against LGIN**. The best score for all variants are marked in **bold** along with LGINs comparable with GIN variants based on a paired t-test with significance level of 10%. Models performing significantly better are marked in **bold** with an asterisk. Evaluation standard defined as per (Xu et al., 2018)

Datasets	MUTAG	PROTEINS	PTC	NCI1
# graphs	188	1113	344	4110
# classes	2	2	2	2
Avg # nodes	17.9	39.1	25.5	29.8
WL subtree	90.4 ± 5.7	75.0 ± 3.1	59.9 ± 4.3	86.0 ± 1.8*
DCNN	67.0	61.3	56.6	62.6
PATCHYSAN	92.6 ± 4.2*	75.9 ± 2.8	60.0 ± 4.8	78.6 ± 1.9
DGCNN	85.8	75.5	58.6	74.4
AWL	87.9 ± 9.8	-	-	-
SUM-MLP (GIN-0)	89.4 ± 5.6	76.2 ± 2.8	64.6 ± 7.0	82.7 ± 1.7
SUM-MLP (GIN- ϵ)	89.0 ± 6.0	75.9 ± 3.8	63.7 ± 8.2	82.7 ± 1.6
SUM-1-LAYER	90.0 ± 8.8	76.2 ± 2.6	63.1 ± 5.7	82.0 ± 1.5
MEAN-MLP	83.5 ± 6.3	75.5 ± 3.4	66.6 ± 6.9	80.9 ± 1.8
MEAN-1-LAYER (GCN)	85.6 ± 5.8	76.0 ± 3.2	64.2 ± 4.3	80.2 ± 2.0
MAX-MLP	84.0 ± 6.1	76.0 ± 3.2	64.6 ± 10.2	77.8 ± 1.3
MAX-1-LAYER (GraphSAGE)	85.1 ± 7.6	75.9 ± 3.2	63.9 ± 7.7	77.7 ± 1.5
SUM-Lorentz (LGIN Variable Curvature)	88.1 ± 5.0	79.1 ± 4.4*	68.2 ± 5.1*	82.3 ± 1.5
SUM-Lorentz (LGIN Fixed Curvature)	90.6 ± 3.9	76.9 ± 2.5	68.4 ± 5.2*	83.2 ± 1.6

model hierarchical relationships by leveraging Lorentzian geometry. Overall, the results demonstrate that incorporating curvature into Graph Isomorphism Networks enhances representational capacity, enabling more effective learning across diverse graph structures.

5.2.2 Performance on Enzymes, Proteins and DD against state of the art graph neural networks

Table 2 presents the detailed performance analysis across the Proteins, Enzymes, and DD datasets. We evaluate multiple models, including Euclidean GNNs and hyperbolic GNN baselines (HGNN and H2H-GCN), alongside our proposed methods LGIN Variable and LGIN Fixed. On the **Enzymes** dataset, our LGIN Fixed model achieves the highest test accuracy of **71.500%**, significantly outperforming the hyperbolic baselines HGNN (51.3%) and H2H-GCN (61.3%), and other Euclidean models. GAT achieves the second best performance (68.500%). The LGIN Variable variant follows closely with 67.380%. For the **DD** dataset, the hyperbolic baseline H2H-GCN achieves the highest test accuracy of **78.2%**. GAT is the second best at 75.900%. HGNN performs very close to GAT (75.8%). Our LGIN Variable model achieves a test accuracy of 73.730%, performing comparably to HGNN and better than many Euclidean baselines, and is the fourth best overall on this dataset. LGIN Fixed has lower performance on DD (70.300%). In the **Proteins** dataset, our LGIN Variable model attains the highest accuracy at **79.100%**, surpassing both LGIN Fixed (76.900%) and the hyperbolic baselines HGNN (73.7%) and H2H-GCN (74.4%). H2H-GCN achieves the third best performance on this dataset. Overall, the results demonstrate that LGIN models remain highly competitive across these datasets. LGIN Fixed is the top performer on Enzymes, while LGIN Variable leads on Proteins. Although H2H-GCN is the best on DD, LGIN Variable and Fixed show strong performance on Proteins and Enzymes respectively, highlighting LGIN’s ability to model complex graph structures effectively within the Lorentzian geometry, competing well against both Euclidean and other hyperbolic methods.

5.2.3 Performance on MoleculeNet Datasets

Table 3 presents the performance analysis of our framework on the MoleculeNet datasets, comparing it against various baseline models, including GAT, GIN, and DGN, as well as their enhanced versions incorporating ECFP and MFP features. Results are reported across three datasets: BACE, BBBP, and HIV.

Table 2: **Detailed Analysis on Proteins, Enzymes and DD.** The best accuracy on the test splits are marked in **bold** while the second best score is underlined. Hyphen indicates the scores were not reported by the authors. Hyperbolic GNN baselines have been marked with an asterisk(*).

Model	L	Test Acc. \pm s.d.	Train Acc. \pm s.d.	#Epoch
ENZYMES				
MLP	4	55.833 \pm 3.516	93.062 \pm 7.551	332.30
<i>vanilla</i> GCN	4	65.833 \pm 4.610	97.688 \pm 3.064	343.00
GraphSage	4	65.000 \pm 4.944	100.000 \pm 0.000	294.20
MoNet	4	63.000 \pm 8.090	95.229 \pm 5.864	333.70
GAT	4	<u>68.500\pm5.241</u>	100.000 \pm 0.000	299.30
GatedGCN	4	65.667 \pm 4.899	99.979 \pm 0.062	316.80
GIN	4	65.333 \pm 6.823	100.000 \pm 0.000	402.10
RingGNN	2	18.667 \pm 1.795	20.104 \pm 2.166	337.30
3WLGNN	3	61.000 \pm 6.799	98.875 \pm 1.571	381.80
HGNN*	-	51.300 \pm 6.100	-	-
H2H-GCN*	-	61.300 \pm 4.900	-	-
LGIN Variable c (Ours)	3	67.380 \pm 4.100	100.000 \pm 0.000	500.00
LGIN Fixed c (Ours)	3	71.500\pm1.600	100.000 \pm 0.000	500.00
DD				
MLP	4	72.239 \pm 3.854	73.816 \pm 1.015	371.80
<i>vanilla</i> GCN	4	72.758 \pm 4.083	100.000 \pm 0.000	266.70
GraphSage	4	73.433 \pm 3.429	75.289 \pm 2.419	267.20
MoNet	4	71.736 \pm 3.365	81.003 \pm 2.593	252.60
GAT	4	<u>75.900\pm3.824</u>	95.851 \pm 2.575	201.60
GatedGCN	4	72.918 \pm 2.090	82.796 \pm 2.242	300.70
GIN	4	71.910 \pm 3.873	99.851 \pm 0.136	275.70
RingGNN	2	-	-	-
3WLGNN	3	-	-	-
HGNN*	-	75.800 \pm 3.300	-	-
H2H-GCN*	-	78.200\pm3.300	-	-
LGIN Variable c (Ours)	3	73.730 \pm 3.200	100.000 \pm 0.000	297.00
LGIN Fixed c (Ours)	3	70.300 \pm 3.500	100.000 \pm 0.000	281.00
PROTEINS				
MLP	4	75.644 \pm 2.681	79.847 \pm 1.551	244.20
<i>vanilla</i> GCN	4	76.098 \pm 2.406	81.387 \pm 2.451	350.90
GraphSage	4	75.289 \pm 2.419	85.182 \pm 3.489	245.40
MoNet	4	76.452 \pm 2.898	78.206 \pm 0.548	306.10
GAT	4	76.277 \pm 2.410	83.186 \pm 2.000	344.10
GatedGCN	4	76.363 \pm 2.904	79.471 \pm 0.695	293.80
GIN	4	74.117 \pm 3.357	75.351 \pm 1.267	420.90
RingGNN	2	67.564 \pm 7.551	67.564 \pm 7.551	450.10
3WLGNN	3	61.712 \pm 4.859	62.427 \pm 4.548	211.40
HGNN*	-	73.700 \pm 2.300	-	-
H2H-GCN*	-	74.400 \pm 3.000	-	-
LGIN Variable c (Ours)	3	79.100\pm4.400	81.750 \pm 10.030	1000.00
LGIN Fixed c (Ours)	3	<u>76.900\pm2.500</u>	84.180 \pm 5.530	700.00

Our method achieves state-of-the-art performance on multiple datasets. Specifically, on the BBBP dataset, **LGIN Fixed c** achieves the highest score of **91.54**, outperforming all other models, while **LGIN Variable c** secures the second-best score of 89.08. On the BACE dataset, **DGCL** achieves the best performance with **91.48**, closely followed by **LGIN Variable c** with 90.30, surpassing the performance of GIN-based models

Table 3: **Analysis of our framework’s performance on MoleculeNet baselines.** The best score is marked in **bold** and the second best score is underlined. GIN models have been marked with an asterisk to indicate that our proposed model significantly outperforms GIN baselines. Hyphen indicates OOM on an 8GB M2 Macbook Pro.

Datasets	BACE	BBBP	HIV
#Molecule	1513	2039	41127
#Tasks	1	1	1
GAT	83.60	65.48	69.26
GIN	73.38*	61.25*	60.33*
DGN	79.88	65.01	75.63
GAT-ECFP	<u>90.99</u>	67.71	75.14
GIN-ECFP	82.84*	64.36*	54.92*
DGN-ECFP	89.56	64.17	73.19
GAT-MFP	89.84	71.70	<u>76.47</u>
GIN-MFP	82.03*	71.04*	62.68*
DGCL	91.48	73.78	81.49
LGIN Variable c (Ours)	90.30	<u>89.08</u>	-
LGIN Fixed c (Ours)	86.56	91.54	73.27

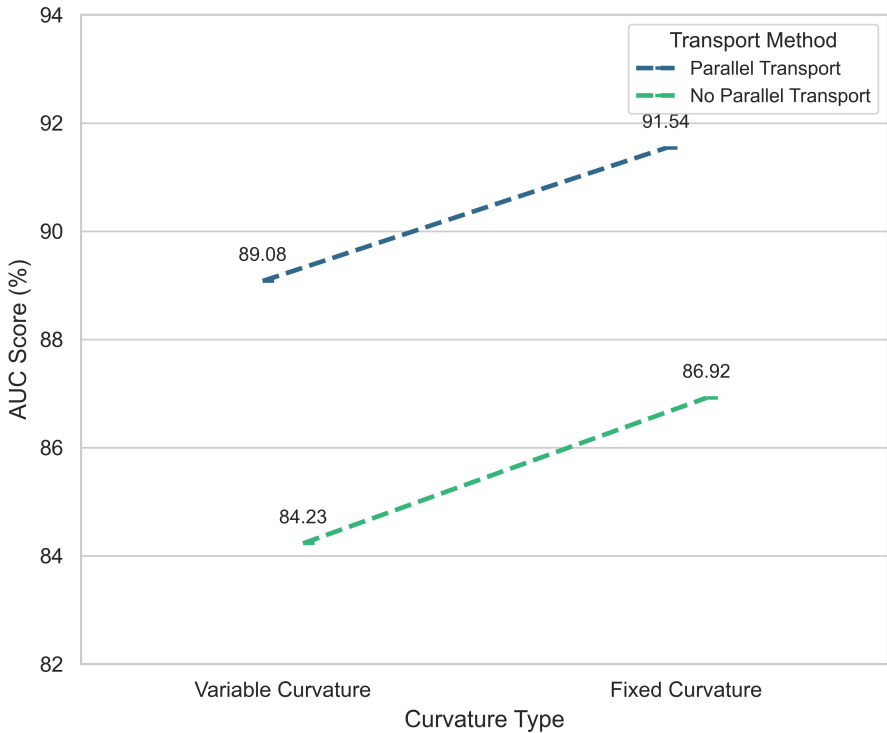


Figure 1: Abalation Study on Curvature Type and Parallel Transport on BBBP

such as GIN-ECFP (82.84*) and GIN-MFP (82.03*). Similarly, for the HIV dataset, **DGCL** attains the highest score of **81.49**, with **GAT-MFP** achieving the second-best score of 76.47.

Furthermore, our LGIN models consistently outperform the baseline GIN models across all datasets, demonstrating the effectiveness of leveraging Lorentzian geometry for molecular representation learning. These results highlight the robustness of our approach in capturing complex molecular structures, thereby achieving superior performance in molecular property prediction tasks.

5.2.4 Empirical Analysis on Curvature and Parallel Transport

In this section, we provide an ablation study on parallel transport and curvatures on the BBBP dataset. As mentioned earlier, in eq.18, we use parallel transport between 2 tangent spaces to ensure geometric consistency and numerical stability. We perform an analysis by considering the following equation i.e eq.21 as well, and show the importance of parallel transport by measuring the performance difference.

$$\mathbf{x}^{\mathcal{L}^k} = \text{LT}^k(\exp_o^c((1 + \epsilon^k) \cdot \log_o^c(\mathbf{x}^{\mathcal{L}^{k-1}}) + \log_o^c(T(\mathbf{x}^{\mathcal{L}^{k-1}})))) \quad (21)$$

figure 1 represents the AUC scores for curvature and parallel transport modes while provides a direct comparison between the results of the two update rules. As noted, cases where parallel transport is employed to the first term of eq.21 perform considerably better. We hypothesize that this is probably due to the fact that parallel transport aligns embeddings which were otherwise distorted due to aggregation, despite all transformations taking place with respect to the origin. With respect to curvature type, there is no significant difference between fixed and variable curvature models, in line with evaluations described in previous sections and (Zhang et al., 2021a).

6 Conclusion and Limitations

In this paper, we address the need for simple yet effective graph neural networks on hyperbolic manifolds capable of capturing both semantic and structural features. We propose the Lorentzian Graph Isomorphic Network (LGIN), which, to the best of our knowledge, is the first framework to extend graph isomorphism tests to hyperbolic spaces with variable and fixed curvature. Through extensive experiments, we demonstrate that LGIN consistently matches or surpasses state-of-the-art models across multiple graph benchmarks. Additionally, we provide a detailed explanation of our update rule, including rigorous derivations for each step, thereby establishing a framework for an approximate solution for the expressivity bottleneck on hyperbolic spaces.

However, our analysis does not offer a comprehensive framework for hyperbolic graph neural networks that directly map between hyperbolic spaces without relying on tangent space projections. Further investigation is required to develop such transformations and fully explore the potential of these models, which we leave as a direction for future research.

References

- Tal Amir, Steven Gortler, Ilai Avni, Ravina Ravina, and Nadav Dym. Neural injective functions for multisets, measures and graphs via a finite witness theorem. *Advances in Neural Information Processing Systems*, 36:42516–42551, 2023.
- Liming Bao, Yan Wang, Xiaoyu Song, and Tao Sun. Hgcge: hyperbolic graph convolutional networks-based knowledge graph embedding for link prediction. *Knowledge and Information Systems*, 67(1):661–687, 2025.
- Gary Bécigneul and Octavian-Eugen Ganea. Riemannian adaptive optimization methods. *arXiv preprint arXiv:1810.00760*, 2018.
- Narendra Choudhary, Nikhil Rao, and Chandan Reddy. Hyperbolic graph neural networks at scale: A meta learning approach. *Advances in Neural Information Processing Systems*, 36:44488–44501, 2023.
- Xingcheng Fu, Jianxin Li, Jia Wu, Jiawen Qin, Qingyun Sun, Cheng Ji, Senzhang Wang, Hao Peng, and Philip S Yu. Adaptive curvature exploration geometric graph neural network. *Knowledge and Information Systems*, 65(5):2281–2304, 2023.
- Will Hamilton, Zhitao Ying, and Jure Leskovec. Inductive representation learning on large graphs. *Advances in neural information processing systems*, 30, 2017.
- Asela Hevopathige and Qing Wang. Uplifting the expressive power of graph neural networks through graph partitioning. *arXiv preprint arXiv:2312.08671*, 2023.

-
- Mehrdad Khatir, Nurendra Choudhary, Sutanay Choudhury, Khushbu Agarwal, and Chandan K Reddy. A unification framework for euclidean and hyperbolic graph neural networks. *arXiv preprint arXiv:2206.04285*, 2022.
- Thomas N Kipf and Max Welling. Semi-supervised classification with graph convolutional networks. *arXiv preprint arXiv:1609.02907*, 2016.
- Xiao Li, Li Sun, Mengjie Ling, and Yan Peng. A survey of graph neural network based recommendation in social networks. *Neurocomputing*, 549:126441, 2023.
- Brian Godwin Lim, Galvin Brice Lim, Renzo Roel Tan, and Kazushi Ikeda. Contextualized messages boost graph representations. *arXiv preprint arXiv:2403.12529*, 2024.
- Qi Liu, Maximilian Nickel, and Douwe Kiela. Hyperbolic graph neural networks. *Advances in neural information processing systems*, 32, 2019.
- Bruno Martelli. An introduction to geometric topology. *arXiv preprint arXiv:1610.02592*, 2016.
- Christopher Morris, Martin Ritzert, Matthias Fey, William L Hamilton, Jan Eric Lenssen, Gaurav Rattan, and Martin Grohe. Weisfeiler and leman go neural: Higher-order graph neural networks. In *Proceedings of the AAAI conference on artificial intelligence*, volume 33, pp. 4602–4609, 2019.
- Hugo Ramirez, Davide Tabarelli, Arianna Brancaccio, Paolo Belardinelli, Elisabeth B Marsh, Michael Funke, John C Mosher, Fernando Maestu, Mengjia Xu, and Dimitrios Pantazis. Fully hyperbolic neural networks: A novel approach to studying aging trajectories. *IEEE Journal of Biomedical and Health Informatics*, 2025.
- Petar Veličković, Guillem Cucurull, Arantxa Casanova, Adriana Romero, Pietro Lio, and Yoshua Bengio. Graph attention networks. *arXiv preprint arXiv:1710.10903*, 2017.
- Zhenqin Wu, Bharath Ramsundar, Evan N Feinberg, Joseph Gomes, Caleb Geniesse, Aneesh S Pappu, Karl Leswing, and Vijay Pande. Moleculenet: a benchmark for molecular machine learning. *Chemical science*, 9(2):513–530, 2018.
- Zhenxing Wu, Dejun Jiang, Chang-Yu Hsieh, Guangyong Chen, Ben Liao, Dongsheng Cao, and Tingjun Hou. Hyperbolic relational graph convolution networks plus: a simple but highly efficient qsar-modeling method. *Briefings in Bioinformatics*, 22(5):bbab112, 2021.
- Yu Xie, Yanfeng Liang, Maoguo Gong, A Kai Qin, Yew-Soon Ong, and Tiantian He. Semisupervised graph neural networks for graph classification. *IEEE Transactions on Cybernetics*, 53(10):6222–6235, 2022.
- Keyulu Xu, Weihua Hu, Jure Leskovec, and Stefanie Jegelka. How powerful are graph neural networks? *arXiv preprint arXiv:1810.00826*, 2018.
- Pinar Yanardag and SVN Vishwanathan. Deep graph kernels. In *Proceedings of the 21th ACM SIGKDD international conference on knowledge discovery and data mining*, pp. 1365–1374, 2015.
- Zi Ye, Yogan Jaya Kumar, Goh Ong Sing, Fengyan Song, and Junsong Wang. A comprehensive survey of graph neural networks for knowledge graphs. *IEEE Access*, 10:75729–75741, 2022.
- Seongjun Yun, Seoyoon Kim, Junhyun Lee, Jaewoo Kang, and Hyunwoo J Kim. Neo-gnns: Neighborhood overlap-aware graph neural networks for link prediction. *Advances in Neural Information Processing Systems*, 34:13683–13694, 2021.
- Shuo Zhang and Lei Xie. Improving attention mechanism in graph neural networks via cardinality preservation. In *IJCAI: proceedings of the conference*, volume 2020, pp. 1395, 2020.
- Yiding Zhang, Xiao Wang, Chuan Shi, Nian Liu, and Guojie Song. Lorentzian graph convolutional networks. In *Proceedings of the web conference 2021*, pp. 1249–1261, 2021a.

Zaixi Zhang, Qi Liu, Hao Wang, Chengqiang Lu, and Chee-Kong Lee. Motif-based graph self-supervised learning for molecular property prediction. *Advances in Neural Information Processing Systems*, 34:15870–15882, 2021b.

Tianxiang Zhao, Xiang Zhang, and Suhang Wang. Graphsmote: Imbalanced node classification on graphs with graph neural networks. In *Proceedings of the 14th ACM international conference on web search and data mining*, pp. 833–841, 2021.

Zihong Zhu, Weiyu Zhang, Xinchao Guo, and Xinxiao Qiao. Lorentzian graph convolution networks for collaborative filtering. In *2023 International Joint Conference on Neural Networks (IJCNN)*, pp. 1–8. IEEE, 2023.

A Proof of Theorem 4.1

Proof. Assume, for contradiction, that such a diffeomorphism $f : \mathcal{M} \rightarrow \mathcal{M}$ exists, satisfying:

$$f^*g = g \quad \text{and} \quad f \circ \Phi(G_1) = \Phi(G_2)$$

Since \mathcal{M} is a Lorentzian manifold with constant negative curvature $c < 0$, it admits a unique global isometry group preserving the Lorentzian metric g . Therefore, any isometry f would map geodesics in \mathcal{M} to geodesics in \mathcal{M} .

By definition, the embeddings $\Phi(G_1)$ and $\Phi(G_2)$ map vertices of G_1 and G_2 into the hyperboloid model of \mathbb{H}^n , such that graph distances are preserved through the Lorentzian distance function. If G_1 and G_2 are non-isomorphic, then there exists no bijection between their vertex sets preserving adjacency and distances.

However, the existence of such an f implies that the embeddings $\Phi(G_1)$ and $\Phi(G_2)$ are related by an isometry, contradicting the assumption that G_1 and G_2 are non-isomorphic. Hence, no such f exists.

$$\therefore \Phi(G_1) \neq f \circ \Phi(G_2) \text{ for any isometry } f$$

□

B Proof of Proposition 4.2

Proof. Let the transformation be denoted by $F(x^\mathcal{L}) = \mathbf{W} \otimes_c^\mathcal{L} x^\mathcal{L}$. We can decompose F into a sequence of maps: $F = f_5 \circ f_4 \circ f_3 \circ f_2 \circ f_1$, where:

1. $f_1 : \mathcal{H}^n \rightarrow T_o\mathcal{H}^n$, $f_1(x^\mathcal{L}) = \log_o^c(x^\mathcal{L})$. The logarithmic map centered at the origin o of the hyperboloid model \mathcal{H}^n is a global diffeomorphism from \mathcal{H}^n (the upper sheet) to $T_o\mathcal{H}^n$. As a diffeomorphism, f_1 is bijective and thus injective.
2. $f_2 : T_o\mathcal{H}^n \rightarrow \mathbb{R}^n$, $f_2(\mathbf{c}v) = \mathbf{c}v_{[1:n]}$. In the hyperboloid model embedded in \mathbb{R}^{n+1} , the tangent space at the origin $o = (1, 0, \dots, 0)$ consists of vectors $\mathbf{c}v = (v_0, v_1, \dots, v_n) \in \mathbb{R}^{n+1}$ such that $\langle o, \mathbf{c}v \rangle_\eta = -1 \cdot v_0 + \sum_{i=1}^n 0 \cdot v_i = -v_0 = 0$. Thus $T_o\mathcal{H}^n = \{(0, v_1, \dots, v_n) \mid v_i \in \mathbb{R}\}$. The map f_2 extracts the spatial components (v_1, \dots, v_n) , providing an isomorphism between $T_o\mathcal{H}^n$ and \mathbb{R}^n . As an isomorphism, f_2 is bijective and thus injective.
3. $f_3 : \mathbb{R}^n \rightarrow \mathbb{R}^d$, $f_3(\mathbf{c}y) = \mathbf{W}\mathbf{c}y$. This is a standard linear transformation. A linear transformation f_3 is injective if and only if its null space, $\ker(\mathbf{W}) = \{\mathbf{c}y \in \mathbb{R}^n \mid \mathbf{W}\mathbf{c}y = \mathbf{c}0\}$, contains only the zero vector. By the Rank-Nullity Theorem ($n = \dim(\ker(\mathbf{W})) + \text{rank}(\mathbf{W})$), this is equivalent to $\text{rank}(\mathbf{W}) = n$. The maximum possible rank for $\mathbf{W} \in \mathbb{R}^{d \times n}$ is $\min(d, n)$. Thus, having rank n requires $d \geq n$. f_3 is injective if and only if \mathbf{W} has full column rank (n).
4. $f_4 : \mathbb{R}^d \rightarrow T_o\mathcal{H}^d$, $f_4(\mathbf{c}z) = (0, \mathbf{c}z)$. Similar to f_2 , this map takes a vector $\mathbf{c}z \in \mathbb{R}^d$ and forms a vector $(0, z_1, \dots, z_d) \in \mathbb{R}^{d+1}$, which lies in $T_o\mathcal{H}^d$. This map is an isomorphism between \mathbb{R}^d and $T_o\mathcal{H}^d$. As an isomorphism, f_4 is bijective and thus injective.

5. $f_5 : T_o\mathcal{H}^d \rightarrow \mathcal{H}^d$, $f_5(\mathbf{c}u) = \exp_o^c(\mathbf{c}u)$. The exponential map centered at the origin o is a global diffeomorphism from $T_o\mathcal{H}^d$ to \mathcal{H}^d (the upper sheet). As a diffeomorphism, f_5 is bijective and thus injective.

The composite function $F = f_5 \circ f_4 \circ f_3 \circ f_2 \circ f_1$ is injective if and only if all functions in the composition are injective. We have shown that f_1, f_2, f_4 , and f_5 are injective. Therefore, F is injective if and only if f_3 is injective.

As shown in point 3, f_3 is injective if and only if the matrix $\mathbf{W} \in \mathbb{R}^{d \times n}$ has full column rank (n). This implies that the output dimension d must be greater than or equal to the input dimension n ($d \geq n$).

Thus, the Lorentzian transformation defined in eq. 14 is injective if and only if \mathbf{W} has full column rank.

To demonstrate this explicitly, assume $F(x_1^{\mathcal{L}}) = F(x_2^{\mathcal{L}})$ for $x_1^{\mathcal{L}}, x_2^{\mathcal{L}} \in \mathcal{H}^n$.

$$\exp_o^c \left(0, \mathbf{W} (\log_o^c x_1^{\mathcal{L}})_{[1:n]} \right) = \exp_o^c \left(0, \mathbf{W} (\log_o^c x_2^{\mathcal{L}})_{[1:n]} \right)$$

Since $f_5 = \exp_o^c$ is injective, we have:

$$\left(0, \mathbf{W} (\log_o^c x_1^{\mathcal{L}})_{[1:n]} \right) = \left(0, \mathbf{W} (\log_o^c x_2^{\mathcal{L}})_{[1:n]} \right)$$

Equating the spatial components (or applying f_4^{-1} which is also injective):

$$\mathbf{W} (\log_o^c x_1^{\mathcal{L}})_{[1:n]} = \mathbf{W} (\log_o^c x_2^{\mathcal{L}})_{[1:n]}$$

Let $\mathbf{c}y_1 = (\log_o^c x_1^{\mathcal{L}})_{[1:n]}$ and $\mathbf{c}y_2 = (\log_o^c x_2^{\mathcal{L}})_{[1:n]}$. Both $\mathbf{c}y_1, \mathbf{c}y_2 \in \mathbb{R}^n$. The equation is $\mathbf{W}\mathbf{c}y_1 = \mathbf{W}\mathbf{c}y_2$. If \mathbf{W} has full column rank, the linear map $f_3(\mathbf{c}y) = \mathbf{W}\mathbf{c}y$ is injective, which implies $\mathbf{c}y_1 = \mathbf{c}y_2$.

$$(\log_o^c x_1^{\mathcal{L}})_{[1:n]} = (\log_o^c x_2^{\mathcal{L}})_{[1:n]}$$

Since f_2^{-1} maps \mathbb{R}^n back to $T_o\mathcal{H}^n$ injectively, this implies the equality of the tangent vectors:

$$\log_o^c x_1^{\mathcal{L}} = \log_o^c x_2^{\mathcal{L}}$$

Finally, since $f_1 = \log_o^c$ is injective, this implies:

$$x_1^{\mathcal{L}} = x_2^{\mathcal{L}}$$

Thus, if \mathbf{W} has full column rank, $F(x_1^{\mathcal{L}}) = F(x_2^{\mathcal{L}})$ implies $x_1^{\mathcal{L}} = x_2^{\mathcal{L}}$, proving F is injective.

Conversely, assume \mathbf{W} does not have full column rank. Since $\mathbf{W} \in \mathbb{R}^{d \times n}$, this means $\text{rank}(\mathbf{W}) < n$. By the Rank-Nullity Theorem, $\dim(\ker(\mathbf{W})) = n - \text{rank}(\mathbf{W}) > 0$. This means there exists a non-zero vector $\mathbf{c}v \in \mathbb{R}^n$ such that $\mathbf{W}\mathbf{c}v = \mathbf{c}0$. Let $\mathbf{c}u = f_2^{-1}(\mathbf{c}v) \in T_o\mathcal{H}^n$. Since f_2^{-1} is injective and $\mathbf{c}v \neq \mathbf{c}0$, $\mathbf{c}u \neq \mathbf{c}0$. Let $x^{\mathcal{L}} = f_1^{-1}(\mathbf{c}u) \in \mathcal{H}^n$. Since f_1^{-1} is injective and $\mathbf{c}u \neq \mathbf{c}0$, $x^{\mathcal{L}} \neq o$. Consider $F(x^{\mathcal{L}})$ and $F(o)$. $F(x^{\mathcal{L}}) = f_5(f_4(f_3(f_2(f_1(x^{\mathcal{L}})))))) = f_5(f_4(f_3(\mathbf{c}u))) = f_5(f_4(\mathbf{W}\mathbf{c}v)) = f_5(f_4(\mathbf{c}0))$. $f_4(\mathbf{c}0) = (0, \mathbf{c}0) \in T_o\mathcal{H}^d$. $F(x^{\mathcal{L}}) = \exp_o^c(0, \mathbf{c}0)$. The exponential map of the zero vector in the tangent space at p is always p . So, $\exp_o^c(0, \mathbf{c}0) = o \in \mathcal{H}^d$. Now consider $F(o)$: $F(o) = \exp_o^c \left(0, \mathbf{W} (\log_o^c o)_{[1:n]} \right)$. $\log_o^c o$ is the zero vector in $T_o\mathcal{H}^n$, which is $(0, \mathbf{c}0) \in \mathbb{R}^{n+1}$. $(\log_o^c o)_{[1:n]} = \mathbf{c}0 \in \mathbb{R}^n$. $F(o) = \exp_o^c(0, \mathbf{W}\mathbf{c}0) = \exp_o^c(0, \mathbf{c}0) = o \in \mathcal{H}^d$. So $F(x^{\mathcal{L}}) = o$ and $F(o) = o$. Since $x^{\mathcal{L}} \neq o$, we have found two distinct points $x^{\mathcal{L}}, o \in \mathcal{H}^n$ that map to the same point $o \in \mathcal{H}^d$. Thus, F is not injective if \mathbf{W} does not have full column rank.

Therefore, the Lorentzian transformation $\mathbf{W} \otimes_c^{\mathcal{L}}$ is injective if and only if the matrix \mathbf{W} has full column rank. \square

C Additional Related Work

(Zhang & Xie, 2020) showed that attention-based GNNs may face limitations in discriminative power due to non-injective aggregation functions. This non-injectivity can lead to different substructures being mapped to the same representation, reducing the model’s effectiveness. To mitigate this, methods have been proposed to enhance injectivity, such as preserving the cardinality information of multisets during aggregation. (Lim et al., 2024) introduced the concept of soft-injective functions. These functions aim to approximate injectivity by ensuring that distinct inputs are mapped to sufficiently different outputs, considering a predefined dissimilarity measure. This approach allows GNNs to maintain discriminative power without necessitating strictly injective aggregation functions.